ARTICLE

OBC
www.rsc.org/obc

# Halo-Derivatised Calix[4]tubes

**Susan E. Matthews,†[a] Vitor Felix,‡[b] Michael G. B. Drew[b] and Paul D. Beer*[a]**

[a] *Inorganic Chemistry Laboratory, Department of Chemistry, University of Oxford, South Parks Road, Oxford, UK OX1 3QR. E-mail: paul.beer@chem.ox.ac.uk; Fax: +44 (0)1865 272690; Tel: +44 (0)1865 272632*

[b] *Department of Chemistry, University of Reading, Whiteknights, Reading, Berks, UK RG6 6AD. E-mail: m.g.b.drew@reading.ac.uk; Fax: +44 (0)118 9316331; Tel: +44 (0)118 9318789*

***Received 18th November 2002, Accepted 17th February 2003***
***First published as an Advance Article on the web 12th March 2003***

Halo functionalisation of calix[4]tubes has been investigated through both derivatisation of individual calix[4]arenes and calix[4]tubes, using classical synthetic methods, to allow preparation of a series of novel derivatives. The solution and solid state properties are in accordance with the constituent calix[4]arenes adopting flattened cone arrangements which on complexation with potassium simplify to a regular cone. Electrospray and $^1$H NMR studies, combined with molecular modelling have been used to ascertain the metal binding of this new series of cryptand like ionophores, demonstrating their retained selectivity for binding potassium over other Group 1 metals and the dependence on counter anion in the weak binding of silver.

## Introduction

Calix[4]tubes, bis calix[4]arenes joined at the lower rim by ethylene linkers, have garnered considerable interest due to their exceptional selectivity for potassium over both Group 1 and 2 metals.[1–6] The rate of this metal complexation can be fine-tuned by the introduction of a variety of alkyl and aryl substituents at the upper-rim of the calix[4]arenes and the preparation of asymmetric calix[4]tubes (Fig. 1) featuring two different calix[4]arene subunits.[2] More recently we have also demonstrated the versatility of the family in its binding of silver ions within the oxygen donor cryptand like cavity[7] and thallium(I) in the arene array.[8]

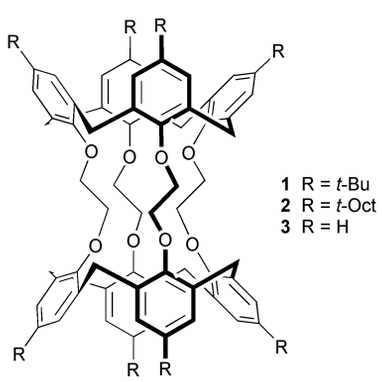


**Fig. 1** Calix[4]tubes.

We were interested in extending the chemistry of calix[4]tubes further in the development of ditopic receptors and metal ion dependent self assembled polymers. Ditopic receptors, in which binding sites are available for both cations and their associated anions, are of interest both in enhancing anion binding through utilisation of the cation charge and in promoting solubilisation and extraction of metal salts.[9] The conformational change in calix[4]tubes on binding of potassium and silver is readily observed by $^1$H NMR and results in a concomitant change in the arene array, in which the calix[4]arenes alter symmetry from $C_{2v}$ to $C_{4v}$. This offers the possibility of development of ditopic receptors based on calix[4]tubes in which selectivity in binding of an anion at an upper-rim binding site is affected allosterically by inclusion of either $K^+$ or $Ag^+$ ions. Equally this structural alteration on cation binding could be exploited in promoting the formation of self assembled hydrogen-bonding polymers based on ureas at the calix[4]tube upper rim.[10]

To this end we were interested in introducing either amino functionality to the calix[4]arenes, for the preparation of upper-rim ureas, or carboxylates for development of amide based anion binding sites. Although a number of synthetic routes to such appended calix[4]arenes have been reported[11] the introduction of halogen substituents is particularly attractive as it enables entry to both desired products. Thus Gabriel methodology can be utilised for conversion of iodo to amino,[12] or lithiation for introduction of carboxylic acids.[13] Additionally such functionalisation opens up the possibility of alkene derivatisation through the Heck reaction.[14]

In this study we report on the suitability of a number of methods for the preparation of halo calix[4]tubes, their structures and their metal ion complexation behaviour using both experimental and theoretical approaches.

## Results and discussion

### Synthesis

Two approaches to the introduction of functionality to the upper rim of calix[4]tubes can be considered. The first, more convergent approach, is to combine two calix[4]arenes (one appended) in the tube forming step, whilst the second relies on regioselective reactions of asymmetric calix[4]tubes (Fig. 2).

Initial studies focused on the introduction of substituents prior to tube formation. Two sites are available for such functionalisation and the more remote site (unit A) was chosen in order to affect least the subsequent tube forming step. Bromination of calix[4]arenes has proved readily accessible, using either bromine or *N*-bromosuccinimide (NBS).[15] Standard NBS methodology gave derivative **5** from the calix[4]arene tetratosylate **4**[16] in 80% yield. However, treatment of **5** with calix[4]arene in the presence of potassium carbonate in refluxing

† *Present address*: Department of Chemistry, Trinity College, University of Dublin, Dublin 2 Ireland.
‡ On sabbatical leave from the Departmento de Quimica, Univesidade de Aveiro, P-3810-193, Aveiro, Portugal.

DOI: 10.1039/b211303a

 

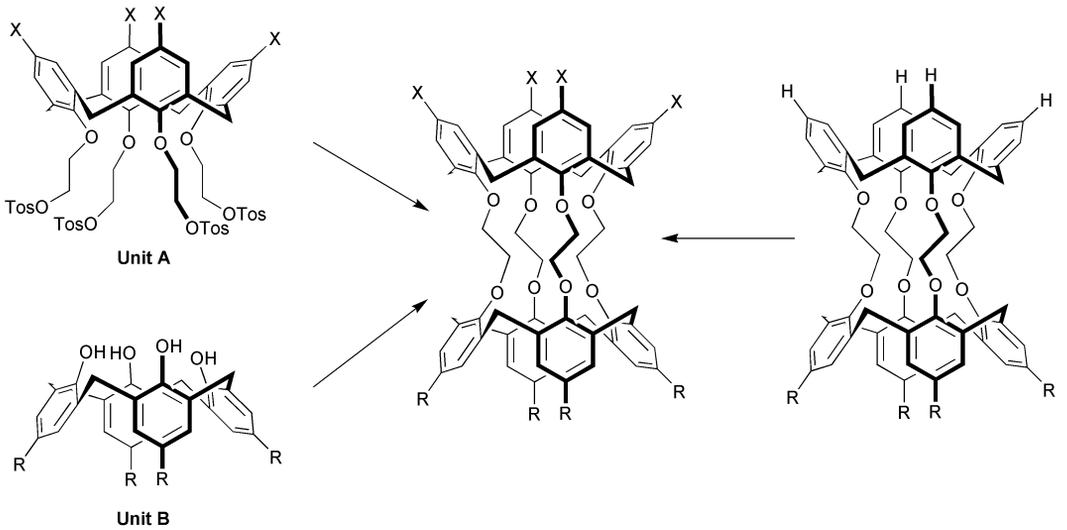


**Fig. 2** Routes to functionalised calix[4]tubes.

xylene, using our standard tube forming conditions,[2] failed to yield the expected calix[4]tube **6** (Scheme 1). A wider range of alkylation conditions including acetonitrile, DMF and mixtures thereof with xylene, were investigated to improve solubility, but proved not conducive to tube formation and no evidence was obtained for the formation of dimer intermediates.

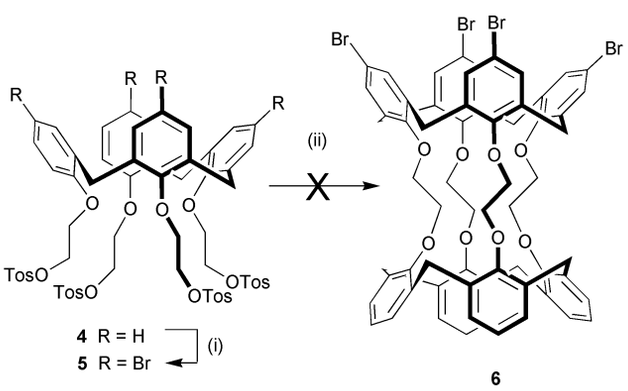


**Scheme 1** *Reagents and conditions*: (i) NBS, *n*-butanone, 24 h, 50 °C. (ii) $K_2CO_3$, xylene, 4 d, reflux.

However, as the calix[4]tube forming reaction has been efficiently optimised to enable efficient preparation of the asymmetric calix[4]tubes **7**, **8** and **9** in excellent yield[2] a second route using post tube formation was investigated.

Bromination of the asymmetric tubes was initially investigated. Treatment of calix[4]tube **7** with NBS in 2-butanone at room temperature for 3 days resulted in an intractable mixture of the di, tri and tetra brominated species.

However, treatment for 5 days at elevated temperature (65 °C) with a large excess of *N*-bromosuccinimide (12 equivalents) proved successful, resulting in the isolation of pure tetra-brominated calix[4]tube **10**, through repeated crystallisation from ethanol, albeit in low yield (18%). The yield could be increased through heating at reflux as shown by the conversion of asymmetric calix[4]tube **7** to the bromo-derivatised calix[4]tube **12** (30%) (Scheme 2).

As bromination proved only low yielding, iodination was also investigated and in contrast was found to allow rapid and high yielding preparation of halo functionalised calix[4]tubes. Treatment of calix[4]tubes **7**, **8** and **9** with iodine in the presence of silver trifluoroacetate in refluxing chloroform[17] gave the respective tetra- and di-iodo derivatives **11**, **13** and **14** in 62–75% yield after only 2 hours (Scheme 2).

The NMR spectra of these halo derivatives show an extreme frozen approximate $C_{2v}$ structure for each calix[4]arene unit and

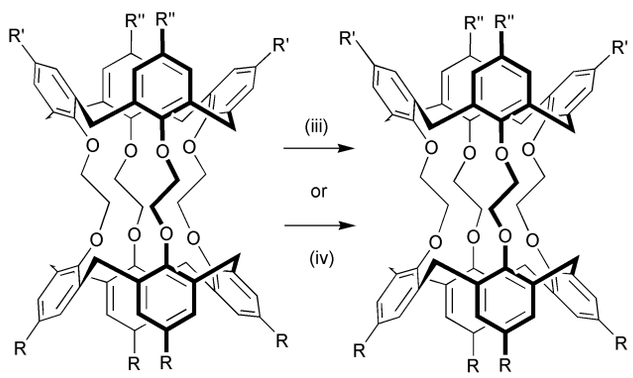


**7** R = *t*-Bu, R' = R'' = H
**8** R = *t*-Oct, R' = R'' = H
**9** R = R' = *t*-Bu, R'' = H

**10** R = *t*-Bu, R' = R'' = Br
**11** R = *t*-Bu, R' = R'' = I
**12** R = *t*-Oct, R' = R'' = Br
**13** R = *t*-Oct, R' = R'' = I
**14** R = R' = *t*-Bu, R'' = I

**Scheme 2** *Reagents and conditions*: (iii) NBS, *n*-butanone, 5 d, 65 °C. (iv) $I_2$, $AgCF_3CO_2$, $CHCl_3$, reflux

a *trans-gauche-trans* arrangement of the ethylene linkers similar to that of the parent calix[4]tubes (Fig. 3). Interconversion of the two equivalent $C_{2v}$ structures through the $C_{4v}$ intermediate is slow; the structure being maintained on heating to 55 °C. However conversion is somewhat faster than for the alkyl calix[4]tubes *e.g.* $K_{obs} = 2.5\ s^{-1}$ (**12**) *cf.* $0.9\ s^{-1}$ (**1**) at 328 K,[18] although considerably slower than the interconversion of the analogous thia calix[4]tube.[3]

In the case of tube **14**, the structure with the iodo units occupying the vertical positions, is the preferred conformer (1.3 : 1) and exchange is, as expected, slower ($1.1\ s^{-1}$ at 328 K) than for the tetra substituted calix[4]tubes. The steric requirements of the iodo groups are greater than for the protons in the parent calix[4]tube accounting for the similarity in energy of the two conformers and the slightly reduced preference between conformers (the ratio of conformers for **9** being 1.6 : 1).[2]

## X-Ray crystallography

The structure of these functionalised calix[4]tubes has been further elucidated by X-ray crystallography. Single crystals of X-ray quality of **11** and **12** were grown from chloroform–methanol–acetone solvent mixtures and the structures of the two calix[4]tubes are shown in Figs. 4 and 5 together with the atomic numbering scheme. The structures can be compared with those of other calix[4]tubes which have been reported, *e.g.* **1**[1] and **2**.[2]

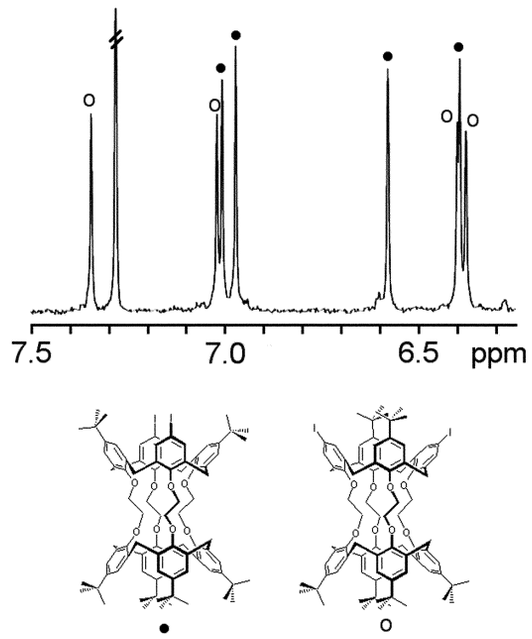


**Fig. 3** Expansion of aromatic region of $^1$H NMR spectrum of **14** showing the relative intensities of the two conformers.

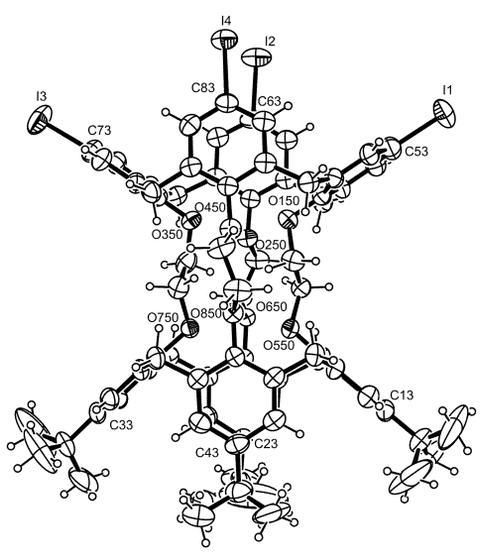


**Fig. 4** The structure of **11** with ellipsoids at 30% probability.

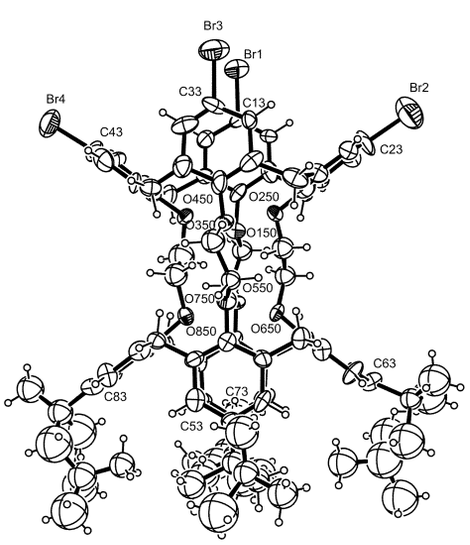


**Fig. 5** The structure of **12** with ellipsoids at 30% probability.

In the calix[4]tubes, the conformation can be quantified by the –O–$CH_2$–$CH_2$–O torsion angles and the angles made by the phenyl rings with the plane of the four linking methylene groups. In **11** and **12**, the four torsion angles are −157.8, −48.2, −157.5 and −40.3° and −153.0, −43.8, −161.8, −40.3° respectively, thus the links contain two *gauche* and two *trans* torsion angles. This type of conformation has been established theoretically[7] as the lowest energy conformation for calix[4]-tubes in the absence of an encapsulated metal, and has also been found in the crystal structures of **1** and **2** where the torsion angles are 161.2, −47.8, −161.2, and 47.8° and −0.5, 161.6, 0.5 and −154.9° respectively although in this latter structure the ethylene link is disordered.

The angles of intersection between the phenyl rings and the four linking methylene groups in **11** are 40.1, 81.7, 43.3 and 87.1° at the *tert*-butyl end of the tube and 34.4, 86.4, 35.0, 83.4° at the iodide end of the tube and in **12** 39.4, 87.9, 35.5, 89.6° at the *tert*-octyl end and 34.6, 86.5, 35.0, 88.7° at the bromide end. These angles show that all the calix[4]arene elements of the calix[4]tubes have the distorted flattened cone conformation with two rings parallel to the tube axis and two rings pseudo-horizontal. Whilst these angles are very similar to those found for **1** and **2** (43.7, 89.6, 41.3, 87.3 and 31.2, 83.2, 37.4, 88.9° respectively within structures with crystallographic centres of symmetry) it is notable that the flattening is more pronounced in the halo calix[4]arene residues. In all cases the *gauche* linkages are bonded to the two phenyl rings that are nearly vertical, parallel to the cage axis, while the *trans* linkages lead to the semi-horizontal phenyl rings.

## Complexation studies

**Potassium binding.** Calix[4]tubes have proved to be some of the most selective potassium complexants over other Group 1 metals known. In this study the complexation behaviour for the Group 1 alkali metals of the synthetic intermediates **10**–**14** has been investigated using a combination of $^1$H NMR and electrospray mass spectrometry techniques. Complexation of potassium is slow on the NMR time scale allowing the kinetic uptake of potassium from potassium iodide, using a solid–liquid extraction method,[9] to be investigated through the concomitant spectral simplification from $C_{2v}$ to $C_{4v}$ (illustrated for **14** in Fig. 6).

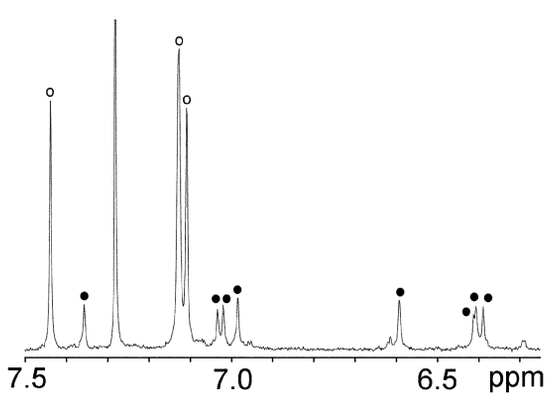


**Fig. 6** Spectrum of **14** after pre-complexation with 20 eq. KI in chloroform–methanol 4 : 1 for 48 h. ○ potassium complex, ● uncomplexed host

A series of quantitative complexation experiments were undertaken in which a 1mM solution (0.5 ml) of a calix[4]tube in chloroform–methanol (4 : 1) was added to 20 eq. (10 μmol) of solid potassium iodide and a NMR spectrum recorded at 1 hour intervals for 15 hours. The uptake of the metal cation could then be measured by direct integration of peaks for complexed and uncomplexed species (Table 1).

**Table 1** % Uptake of potassium by calix[4]tubes after 15 hours[a]

| | |
|---|---|
| **3** | 11% |
| **10** | 6.5% |
| **11** | 3% |
| **12** | 20% |
| **13** | 18% |
| **14** | 42% |

[a] $CDCl_3$–$CD_3OD$ 4 : 1, 20 eq. KI.

Not surprisingly, introduction of the halide residue has a marked effect on the degree of complexation of potassium (Table 1), all new halo-derivatised tubes showing reduced uptake in comparison to their alkyl appended parent tubes.[2] Calix[4]tube **14** featuring only two iodo substituents shows the fastest rate of potassium complexation of the functionalised tube series with more than 40% conversion over 15 hours. However, the *tert*-butyl tetra-bromo and -iodo calix[4]tubes **10** and **11** show only slight uptake over the 15 h observation period, less than for calix[4]tube **3** in which no *para* substituents are present. Although over a longer time span of 9 days more than 10% of these tubes exist as the potassium complex.

When considering the calix[4]tubes which are tetra substituted with halo residues it is interesting to note that the calix[4]tubes featuring *tert*-octyl units are more tolerant to the introduction of halo residues; showing relatively faster kinetic uptake than the corresponding *tert*-butyl tubes. This is in contrast to the results observed with the parent tubes **7** and **8** in which *tert*-butyl calix[4]tubes show faster rates of uptake.[2] Additionally, in all cases the specific halo residue introduced does not significantly alter the rate of potassium uptake, being only slightly faster for the bromo derivatives.

In an attempt to rationalise these findings the proposed mechanism of potassium complexation by calix[4]tubes should first be considered. Extensive NMR complexation studies ($^1$H and $^{205}$Tl), X-ray structural analyses and molecular modelling investigations suggest potassium complexation proceeds *via* an axial route through the calix[4]arene annuli of the tubular structure. The crystal structures of **1**, **2**·$Tl_2^{2+}$ and **1**·$K^+$ shown in Fig. 7 illustrate the three stages in the introduction of metals into the cavity. First in (a), the structure of the calix[4]tube is shown, then as in (b) the metal enters the top of the calixarene and forms an intermediate complex interacting with the aromatic rings and then the metal proceeds into the centre of the calix[4]tube and is complexed by the eight oxygen donor atoms (c).

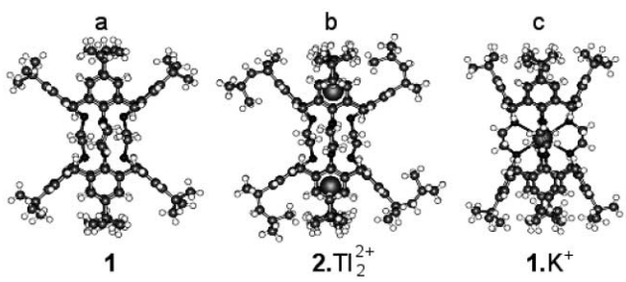


**Fig. 7** The three stages of metal encapsulation within calix[4]tubes illustrated by the crystals structures of **1**, **2**·$Tl_2^{2+}$ and **1**·$K^+$.

In (a), the calix[4]tube has a conformation with alternate O–C–C–O torsion angles *trans* and *gauche* (tgtg). In this particular conformation the central cage composed of eight oxygen atoms cannot form an inclusion complex because of the two *trans* linkages. In (b) the metal ions have entered the calix[4]tube and while the polyether conformations remain the same, the metal ions now interact with the phenyl rings at each end in an intermediate position. In (c) a metal ion has reached the centre of the calix[4]tube and this has been accompanied by a change in conformation of the polyether cage so that all four torsion angles are now *gauche* thus enabling all eight oxygen atoms to bond to the metal ion. Concomitantly the conformations of the individual calix[4]arenes in the calix[4]tube both change to a cone.

As Table 1 illustrates the electron withdrawing halogen substituents of the new halo-derivatised calix[4]tubes serve to disfavour the rate of potassium complexation. Assuming an axial route of entry this suggests that the intermediate π-cation complex will be weaker for the halo-derivatised calix[4]tubes as compared to the *tert*-butyl and *tert*-octyl electron donating substituents of the parent calix[4]tubes. It is noteworthy that with calix[4]tube **11** molecular modelling studies reveal that the potassium cation preferentially enters through the *tert*-butyl end of the tubular structure (*vide supra*).

**Group 1 selectivity studies.** The selectivity of these new members of the calix[4]tube family for potassium over other Group 1 metal ions was also investigated through competitive electrospray mass spectrometry techniques. This approach has recently been developed for study of host–guest complexation as the ions in the gas phase have been demonstrated to reflect accurately the solution situation.[2,19] Pre-treatment of calix[4]tubes **10**–**14** with 20 eq. of each alkali metal iodide in a 4 : 1 chloroform–methanol mixture for 24 hours gave rise to mass spectra in all cases in which the potassium cryptate was the dominant species. Thus demonstrating that introduction of electron withdrawing substituents at the upper rim does not affect the selectivity of calix[4]tubes for potassium complexation.

**Silver binding.** The silver binding properties of these halo-derivatised tubes were also investigated. This is of particular interest given the importance of the counter-ion in binding of the cation[7] and the use of silver during our synthetic studies to promote iodination. Halo calix[4]tubes when treated with 20 eq. of $AgPF_6$ in $CDCl_3$–$CH_3OD$ showed immediate complexation within the cryptand-like cavity as demonstrated by spectral simplification to an approximate $C_{4v}$ symmetry (Fig. 8). It is interesting that the signals are considerably broadened in comparison to those of the potassium complex suggesting a weaker binding process which may involve shuttling between a sub-set of the eight oxygen array. These results are in agreement with our molecular modelling results in which the conformations of the polyether linkages rapidly change even when the metal is bound (*vide supra*).

In contrast, with silver trifluoroacetate under identical conditions, no spectral simplification was observed, demonstrating that the metal ion is not bound within the polyether cavity. No evidence was observed for binding within the arene array; the shifts for arene protons remained identical to those of the parent tube. These results suggest that during the iodination reaction silver is not bound within the oxygen array or the arenes and that the calix[4]tube remains in a $C_{2v}$ symmetrical arrangement with the calix[4]arenes in extreme flattened cones. This is in line with our previous studies with AgI where no binding was observed but in contrast to Stibor and co-workers[4] who have reported binding of silver within the arene array, based on spectral shifts, when the counter-ion is triflate.

**Molecular modelling.** The formation of metal complexes of the tetra iodinated calix[4]tube **11** with the three guest metal ions ($Ag^+$, $K^+$ and $Tl^+$) was also modelled to investigate how the change in substituent from *tert*-butyl to iodine affected the likelihood of metal insertion within the calix[4]tube in comparison to our earlier studies on **1**.[2,7] We were also interested in establishing whether the metal ions were more likely to enter the calix[4]tube through the *tert*-butyl or iodo calix[4]arene annulus.

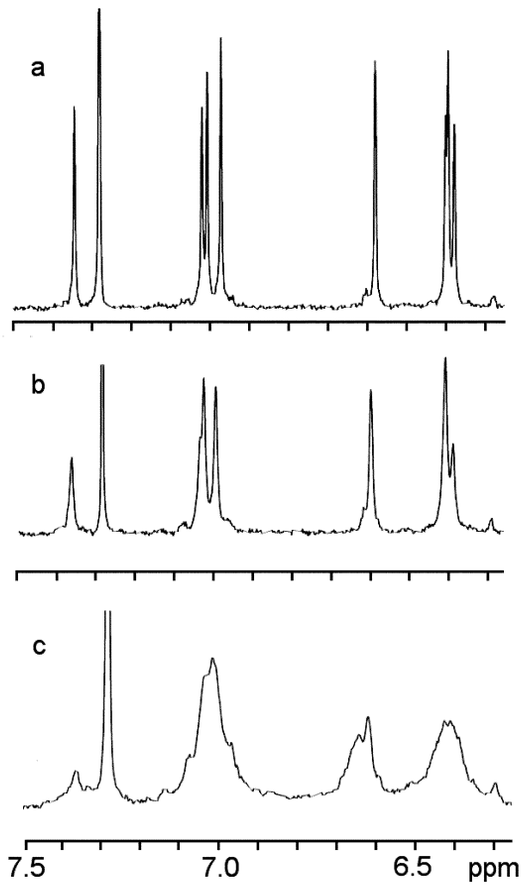


**Fig. 8** Expansion of the aromatic region of the $^1$H NMR of **14** in chloroform–methanol 4 : 1 a) uncomplexed host b) in the presence of 20 eq. of $AgCF_3CO_2$ c) in the presence of 20 eq. of $AgPF_6$.

The simulations were carried out on **11**·$M^+$ using a starting model obtained from the crystal structure of **11**, that is with alternate O–$CH_2$–$CH_2$–O torsion angles *trans* and *gauche*. The metal was positioned inside the calix tube adjacent to the phenyl rings (the intermediate position) first (a) at the *tert*-butyl end and then (b) at the iodo end, and each model was subsequently energy-minimised. The starting models were then subjected to molecular dynamics simulations at a range of temperatures appropriate to the metal included in the simulation; that is at a temperature at which the metal ion does not spontaneously move to the central cavity. The results were characterised *via* plots of the four O–$CH_2$–$CH_2$–O torsion angles against time.

In the case of $K^+$ at 400 K (Fig. 9) during a short period of time, the conformational change *tgtg* ⟶ *tggg* ⟶ *gggg* occurs and concomitantly the metal ion enters into the central cavity of the calix[4]tube. This event occurs at 58 ps in (a) and 390 ps in (b), thus suggesting that the metal ion is more likely to enter the calix[4]tube from the end with the four *tert*-butyl groups rather than the end with the four iodine atoms. This result can be compared with previous simulations in which the $K^+$ ion entered the centre of calix[4]tube **1** at 400 K after 152 ps. In both simulations, apart from the major change in conformation from *trans* to *gauche* of the two O–C–C–O link torsion angles, there is also variation in the sign of the torsion angles. These angles were found to change relatively easily and the various conformations for **11**·$K^+$ were found from energy minimisation to be very similar in energy (gggg, 275.88, gggg, 278.89, ggg$^-$ g$^-$, 279.28, gg$^-$ gg$^-$, 281.55 kcal mol$^{-1}$)

The simulations were then repeated with the smaller ion $Ag^+$. The metal ion rapidly entered the cavity at 300 K with concomitant conformational change from t$^-$ g t$^-$ g to g$^-$ ggg, after 2 ps from the *tert*-butyl side and 15 ps from the iodide side (Fig. 10).

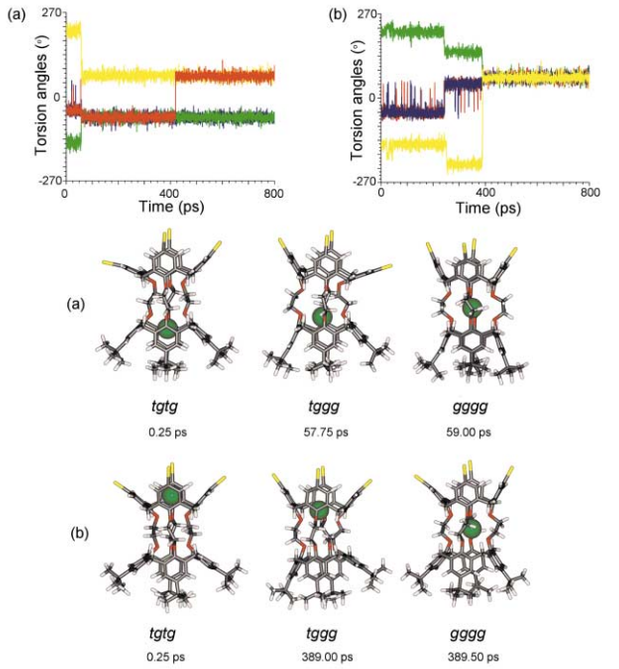


**Fig. 9** Plot of the four O–C–C–O torsion angles during the 800 ps simulation for **11**·$K^+$ at 400 K and snapshots showing changes in conformations. (a) shows the metal starting at the tetra-*tert*-butyl end and (b) the metal starting at the tetraiodide end.[20,21]

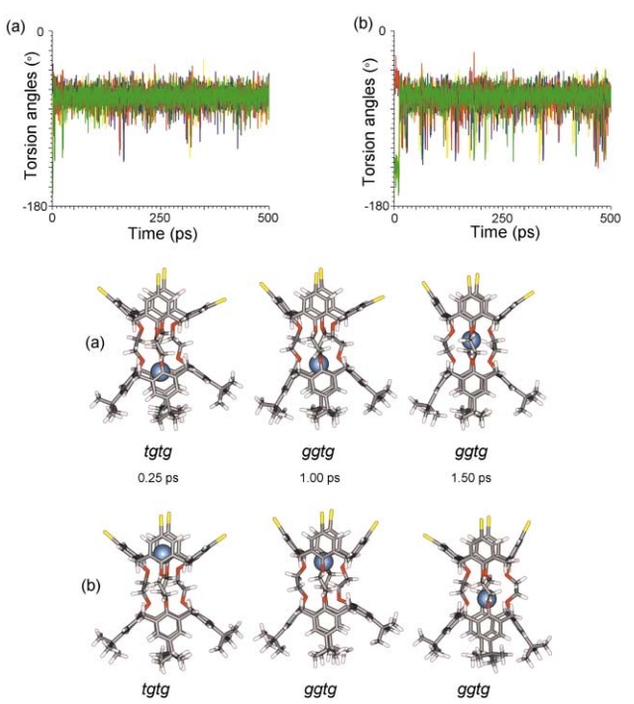


**Fig. 10** Plot of the four O–C–C–O torsion angles during the 500 ps simulation for **11**·$Ag^+$ at 300 K and snapshots of the relevant events (or conformations). (a) shows the metal starting at the *tert*-butyl end and (b) the metal starting at the iodide end.[20,21]

However in both cases during the remaining period of the simulation one of the torsion angles changed frequently from *gauche* to *trans* and an alternation of those two conformations is observed suggesting that the macrocyclic cavity is too small to retain the metal centre bonded to all eight oxygen atoms and that the ions enter and leave the cavity rapidly. This is in line with the broad NMR signals observed in our complexation studies with $AgPF_6$.

With the larger $Tl^+$ cation it had been previously observed that the metal only entered the cavity of **1** after 295 ps at 600 K.

However with **11**, in two simulations the metal was found to enter the cavity after 124 and 218 ps respectively from the *tert*-butyl end. However it proved necessary to increase the temperature to 700 K to enable the metal to enter the cavity from the iodide end which it then did after 142 ps (Fig. 11).

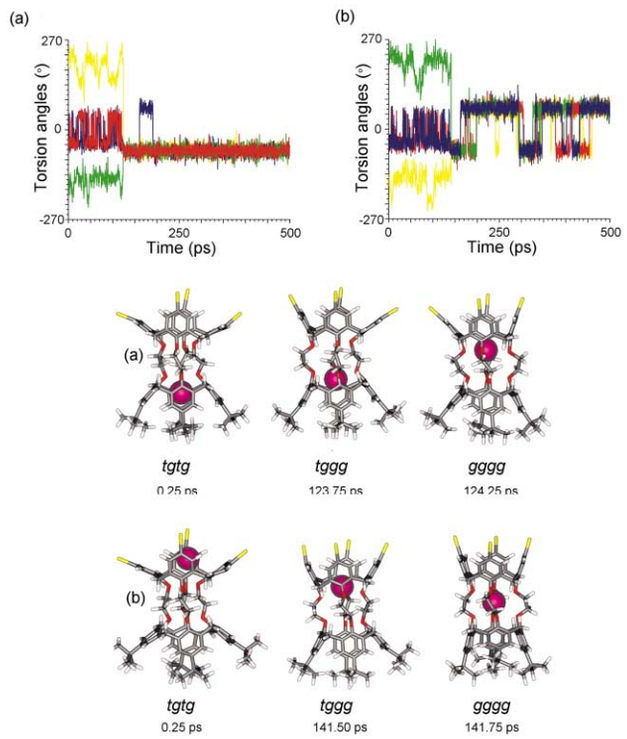


**Fig. 11** Plot of the four O–C–C–O torsion angles during the 500 ps simulation for **11**·$Tl^+$ and snapshots of the relevant events (or conformations). (a) shows the metal starting at the *tert*-butyl end at 600 K and (b) the metal starting at the iodide end at 700 K.[20,21]

From these simulations it is clear that the mechanism of encapsulation of metals within **11** is equivalent to that established for **1** and shown in Fig. 7. However with **11**, as previously discussed there are two possible routes by which the metal can enter the cavity and all our simulations indicate that the metal preferentially enters through the *tert*-butyl end which may be due to the relative stabilities of the π-metal cation intermediate complex. When the metal enters *via* the *tert*-butyl end, the intermediate complex is stabilised by metal phenyl interactions while when the metal enters the calix[4]tube from the end with the four iodine atoms the intermediate complex is relatively weakened as a consequence of the electron withdrawing halo substituents.

## Conclusions

Halogenation, of asymmetric calix[4]tubes, affords rapid entry into the functionalised series **9**–**12**, with iodination proving the most facile approach. Whilst these functionalised tubes retain their selectivity for complexation of potassium over other Group 1 metals, the introduction of halo substituents is detrimental to the complexation rate observed by $^1$H NMR studies. Molecular modelling techniques suggest that destabilisation of the π-metal cation arene bound intermediate due to the electron withdrawing halogen substituents may account for the decreased rate of uptake into the oxygen array. Silver complexation studies demonstrate the role of counter anion in determining the binding mode of the cation. $^1$H NMR studies show unequivocally that silver can bind within the oxygen array, in the case of hexafluorophosphate but not in the case of trifluoroacetate.

## Experimental

All chemicals were commercial grade and used without further purification unless otherwise stated. Solvents were pre-dried, purified by distillation and stored under nitrogen where appropriate. Xylene was stored over calcium hydride and triethylamine was distilled from potassium hydroxide.

Nuclear magnetic resonance spectra were recorded using either a 300 MHz Varian VXWorks spectrometer, a 500 MHz Varian Unity spectrometer or 400 MHz Bruker DPX400 . Electrospray mass spectra were recorded using Micromass LCT equipment and MALDI on a Micromass TofSpec 2E Reflectron MALDI MS.[22]

**Tetrakis[(4-methylphenyl)sulfonyloxyethoxy]-*p*-bromocalix-[4]arene 5.** *N*-Bromosuccinimide (1.5 g, 10.84 mmol) was added to a suspension of calix[4]arene tetra tosylate (1.0 g, 0.82 mmol) in *n*-butanone (20 ml) and the resulting mixture stirred at 50 °C for 24 h. The reaction was quenched with 10% sodium metabisulfite (50 ml) and the organic layer separated, washed with water and dried. Evaporation yielded crude material which was re-crystallised from dichloromethane–ethanol to give **5** as a white solid (1.0 g, 80%).

$^1$H NMR (300 MHz [D]$CHCl_3$ 18 °C): $\delta$ = 2.45 (s, 12H; Ar–C$H_3$), 2.99 (d, $^2J$ = 14 Hz (H, H), 4H; Ar–C$H_2$–Ar), 4.14 (br s, 8 Hz; ArOC$H_2$), 4.28 (d, $^2J$ = 14 Hz (H, H), 4H; Ar–C$H_2$–Ar), 4.37 (br s, $SO_3CH_2$), 6.72 (s, 8H; Ar–*H*), 7.35 (d, $^3J$ = 8 Hz (H, H), 8H, tosyl 2,4), 7.74 (d, $^3J$ = 8 Hz (H, H), 8H, tosyl 3,5); $^{13}$C NMR (75 MHz, [D]$CHCl_3$, 18 °C): $\delta$ = 21.69 (*C*$H_3$ (tosyl)), 30.42 (Ar–*C*$H_2$–Ar), 69.51 ($SO_3$*C*$H_2$), 71.96 (O*C*$H_2$), 116.02 (*Ar*–Br), 127.82 (tosyl 2,4), 129.99 (tosyl 3,5), 131.20 (*Ar*–$H_{(ortho)}$), 132.46 (*Ar*–$CH_3$), 135.94 (*Ar*–$CH_2$), 145.14 (*Ar*–S), 154.14 (*Ar*–O); MS (MALDI): *m*/*z*: 1554.89 [*M* + Na].

**Calix[4]tube 10.** *N*-Bromosuccinimide (0.55 g, 3.06 mmol) was added to a suspension of calix[4]tube **7** (0.30g, 0.26 mmol) in *n*-butanone (10 ml) and the resulting mixture stirred at 65 °C for 5 days. The resulting precipitate was collected and then triturated with ethanol to give a white solid (0.07 g, 18%). $^1$H NMR (300 MHz [D]$CHCl_3$ 18 °C): $\delta$ = 0.80 (s, 18H; (C$H_3$)$_3$), 1.31 (s, 18H; (C$H_3$)$_3$′), 3.24 (d, $^2J$ = 13 Hz (H, H), 4H; Ar–C$H_2$–Ar (Br′)), 3.28 (d, $^2J$ = 11 Hz (H, H), 4H; Ar–C$H_2$–Ar (*t*-Bu′)), 4.39 (s, 8H; OC$H_2$), 4.45 (d, $^2J$ = 13 Hz (H, H), 4H; Ar–C$H_2$–Ar (*t*-Bu)), 4.50 (d, $^2J$ = 14 Hz (H, H), 4H; Ar–C$H_2$–Ar (Br)), 4.92 (m, 4H; OC$H_2$′), 6.50 (s, 4H; Ar–*H* (*t*-Bu)), 6.58 (s, 4H; Ar–*H* (Br)), 7.12 (s, 4H; Ar–*H*(*t*-Bu′)), 7.25 (s, 4H (Br)′); $^{13}$C NMR (75 MHz, [D]$CHCl_3$, 18 °C): $\delta$ = 30.95 ((*C*$H_3$)$_3$), 31.68 ((*C*$H_3$)$_3$′), 31.90 (Ar–*C*$H_2$–Ar), 32.08 (Ar–*C*$H_2$–Ar), 33.55 (*C*H(CH$_3$)$_3$), 34.13 (*C*H(CH$_3$)$_3$′), 72.04 (O*C*$H_2$), 72.32 (O*C*$H_2$(*t*-Bu)′), 72.58 (O*C*$H_2$), 73.18 (O*C*$H_2$ (Br)′), 115.01 (Ar–C(Br)′), 115.65 (*Ar*–C(Br)), 124.99 (Ar–C(*t*-Bu)), 125.62 (*Ar*–C(*t*-Bu)′), 131.07 (Ar–C$_{(ortho)}$(Br)), 131.60 (*Ar*–C$_{(meta)}$-(*t*-Bu)), 131.76 (*Ar*–C$_{(ortho)}$(*t*-Bu)), 134.53 (*Ar*–C$_{(meta)}$(*t*-Bu)), 134.99 (*Ar*–C$_{(meta)}$(Br)), 137.355 (*Ar*–C$_{(meta)}$(Br)), 144.64 (*Ar*–C(*t*-Bu)), 145.17(*Ar*–C(*t*-Bu)′), 152.31 (*Ar*–C$_{(para)}$(*t*-Bu)), 154.21 (*Ar*–C$_{(para)}$(Br)), 155.77 (*Ar*–C$_{(para)}$(*t*-Bu)′), 157.46 (*Ar*–C$_{(para)}$-(Br)′); MS (MALDI): *m*/*z*: 1515.25 [*M* + Na].

**Calix[4]tube 12.** As for synthesis of **4** from calix[4]tube **8** with reaction mixture heated at reflux. Yield = 30%, $^1$H NMR (300 MHz [D]$CHCl_3$ 18 °C): $\delta$ = 0.56 (s, 18H; (C$H_3$)$_3$), 0.80 (s, 26H; (C$H_3$)$_3$′ + (C$H_3$)$_2$), 1.34 (s, 12H; (C$H_3$)$_2$′ + CHC$H_2$), 1.74 (s, 4H; CHC$H_2$(*t*-Oct)′), 3.27 (d, $^2J$ = 14Hz (H, H), 8H; Ar–C$H_2$–Ar (*t*-Oct +Br)), 4.38 (m, 8H; OC$H_2$), 4.48 (d, $^2J$ = 13 Hz (H, H), 4H; Ar–C$H_2$–Ar (*t*-Oct)′), 4.55 (d, $^2J$ = 13 Hz (H, H), 8H; Ar–C$H_2$–Ar (Br)′), 4.99 (m, 4H; OC$H_2$′), 5.17 (m, 4H; OC$H_2$′), 6.49 (s, 4H; Ar–*H* (*t*-Oct)), 6.60 (s, 4H; Ar–*H* (Br)), 7.07 (s, 4H; Ar–*H* (*t*-Oct)′), 7.27 (s, 4H; Ar–*H* (Br)′); $^{13}$C NMR (75 MHz, [D]$CHCl_3$, 18 °C): $\delta$ = 30.81((*C*$H_3$)$_2$ (*t*-Oct)), 31.55 ((*C*$H_3$)$_3$ (*t*-Oct)′), 31.75 ((*C*$H_3$)$_2$ (*t*-Oct)′ + Ar–*C*$H_2$–Ar), 32.19 ((*C*$H_3$)$_3$

(*t*-Oct) + Ar–$CH_2$–Ar), 32.40 ($CH(CH_3)_3$), 32.48 ($CH(CH_3)_3$), 37.53 ($CH(CH_3)_2$), 38.11 ($CH(CH_3)_2'$), 56.79 ($CH_2CH'$), 57.17 ($CH_2CH$), 72.42 ($OCH_2$), 72.74 ($OCH_2$), 73.46 ($OCH_2$(Br)′), 114.98 (*Ar*–C(Br)′), 115.65 (*Ar*–C(Br)), 125.84 (*Ar*–$C_{(ortho)}$(*t*-Oct)), 126.41 (*Ar*–$C_{(ortho)}$(*t*-Oct)′), 131.11 (*Ar*–$C_{(ortho)}$(Br)), 131.18 (*Ar*–$C_{(meta)}$(*t*-Oct)′), 131.78 (*Ar*–$C_{(ortho)}$(Br)′), 134.52 (*Ar*–$C_{(meta)}$(*t*-Oct + Br)), 137.36 (*Ar*–$C_{(meta)}$(Br)′), 143.76 (*Ar*–C(*t*-Oct)′), 144.48 (*Ar*–C(*t*-Oct)), 152.70 (*Ar*–$C_{(para)}$(*t*-Oct)), 154.21 (*Ar*–$C_{(para)}$(Br)), 155.91(*Ar*–$C_{(para)}$(*t*-Oct)′), 157.66-(*Ar*–$C_{(para)}$(Br)′); MS (MALDI): *m*/*z*: 1739.06 [*M* + Na].

**General synthesis of iodocalix[4]tubes.** Calix[4]tube **7**,**8** or **9** (0.14 mmol) in chloroform (15 ml) was added to a refluxing suspension of silver trifluoroacetate (3 eq. per iodo unit) in chloroform (15 ml). The mixture was refluxed for 30 minutes and then an excess of iodine was added until the solution retained a purple colour. After a further 45 minutes at reflux the mixture was cooled and filtered through Celite®. The solution was washed three times with a 10% solution of sodium thiosulfate, water and brine. After removal of the solvent *in vacuo* the pure iodocalix[4]tube was precipitated from chloroform–ethanol.

**Calix[4]tube 11.** Yield = 69%,$^1$H NMR (300 MHz [D]$CHCl_3$ 18 °C): $\delta$ = 0.79 (s, 18H; ($CH_3$)$_3$), 1.30 (s, 18H; ($CH_3$)$_3$′), 3.21 (d, $^2J$ = 14 Hz (H, H), 4H; Ar–$CH_2$–Ar (I′)), 3.23 (d, $^2J$ = 13 Hz (H, H), 4H; Ar–$CH_2$–Ar (*t*-Bu′)), 4.38 (s, 8H; $OCH_2$), 4.43 (d, $^2J$ = 13 Hz (H, H), 8H; Ar–$CH_2$–Ar (*t*-Bu + I)), 4.87 (m, 4H; $OCH_2$′), 5.16 (m, 4H; $OCH_2$′), 6.50 (s, 4H; Ar–*H* (*t*-Bu)), 6.74 (s, 4H; Ar–*H* (I)), 7.12 (s, 4H; Ar–*H* (*t*-Bu′)), 7.43 (s, 4H (I)′); $^{13}$C NMR (75 MHz, [D]$CHCl_3$, 18 °C): $\delta$ = 30.95 (($CH_3$)$_3$), 31.68 (($CH_3$)$_3$′), 31.40 (Ar–$CH_2$–Ar), 32.03 (Ar–$CH_2$–Ar), 33.54 ($CH(CH_3)_3$), 34.12 ($CH(CH_3)_3'$), 72.00 ($OCH_2$), 72.24 ($OCH_2$), 72.51 ($OCH_2$), 73.14 ($OCH_2$), 86.07 (Ar–C(I)′), 86.54 (*Ar*–C(I)), 124.99 (Ar–C(*t*-Bu)), 125.60 (*Ar*–C(*t*-Bu)′), 131.59 (*Ar*–$C_{(meta)}$(*t*-Bu)), 134.95 (*Ar*–$C_{(meta)}$(*t*-Bu + I)), 137.12 (Ar–$C_{(ortho)}$(I)), 137.72 (Ar–$C_{(ortho)}$(I)), 137.89 (*Ar*–$C_{(meta)}$(I)), 144.61 (*Ar*–C(*t*-Bu)), 145.15 (*Ar*–C(*t*-Bu)′), 152.27 (*Ar*–$C_{(para)}$(*t*-Bu)), 155.03 (*Ar*–$C_{(para)}$(I)), 155.75 (*Ar*–$C_{(para)}$(*t*-Bu)′), 158.28 (*Ar*–$C_{(para)}$(I)′); MS (MALDI): *m*/*z*: 1702.84 [*M* + Na].

**Calix[4]tube 13.** Yield = 75%, $^1$H NMR (300 MHz [D]$CHCl_3$ 18 °C): $\delta$ = 0.55 (s, 18H; ($CH_3$)$_3$), 0.79 (s, 26H; ($CH_3$)$_3$′ + ($CH_3$)$_2$), 1.34 (s, 12H; ($CH_3$)$_2$′ + $CHCH_2$), 1.74 (s, 4H; $CHCH_2$(*t*-Oct)′), 3.21 (d, $^2J$ = 13 Hz (H, H), 4H; Ar–$CH_2$–Ar(I)), 3.23 (d, $^2J$ = 13 Hz (H, H), 4H; Ar–$CH_2$–Ar (*t*-Oct)), 4.33 (m, 4H; $OCH_2$), 4.35 (m, 4H; $OCH_2$), 4.43 (d, $^2J$ = 13 Hz (H, H), 4H; Ar–$CH_2$–Ar (*t*-Oct)′), 4.46 (d, $^2J$ = 13 Hz (H, H), 4H; Ar–$CH_2$–Ar (I)′), 4.92 (m, 4H; $OCH_2$′), 5.18 (m, 4H; $OCH_2$′), 6.49 (s, 4H; Ar–*H*(*t*-Oct)), 6.76 (s, 4H; Ar–*H* (Br)), 7.24 (s, 4H; Ar–*H* (*t*-Oct)′), 7.45 (s, 4H; Ar–*H* (Br)′); $^{13}$C NMR (75 MHz, [D]$CHCl_3$, 18 °C): $\delta$ = 30.80 (($CH_3$)$_2$ (*t*-Oct)), 31.40 (Ar–$CH_2$–Ar), 31.53 (($CH_3$)$_3$ (*t*-Oct)′), 31.74 (($CH_3$)$_2$ (*t*-Oct)′ + Ar–$CH_2$–Ar), 32.19 (($CH_3$)$_3$ (*t*-Oct) + ($CH(CH_3)_3$), 32.40 ($CH(CH_3)_3$), 37.52 ($CH(CH_3)_2$), 38.11 ($CH(CH_3)_2'$), 56.76 ($CH_2CH'$), 57.17 ($CH_2CH$), 72.42 ($OCH_2$), 72.66 ($OCH_2$), 73.43 ($OCH_2$(I)′), 86.04 (*Ar*–C(I)′), 86.54 (*Ar*–C(I)), 125.84 (*Ar*–$C_{(ortho)}$(*t*-Oct)), 126.39 (*Ar*–$C_{(ortho)}$(*t*-Oct)′), 131.17 (*Ar*–$C_{(meta)}$(*t*-Oct)′), 134.52 (*Ar*–$C_{(meta)}$(I)), 134.94 (*Ar*–$C_{(meta)}$(*t*-Oct)), 137.16 (*Ar*–$C_{(ortho)}$(I)′), 137.75 (*Ar*–$C_{(meta)}$(I)′), 137.90 (*Ar*–$C_{(meta)}$(I)′), 143.72 (*Ar*–C(*t*-Oct)′), 144.48 (*Ar*–C(*t*-Oct)), 152.67 (*Ar*–$C_{(para)}$(*t*-Oct)), 155.04 (*Ar*–$C_{(para)}$(I)), 155.92 (*Ar*–$C_{(para)}$-(*t*-Oct)′), 158.52 (*Ar*–$C_{(para)}$(I)′); MS (MALDI): *m*/*z*: 1927.88 [*M* + Na].

**Calix[4]tube 14 (Fig. 12).** Yield = 62%, $^1$H NMR (300 MHz [D]$CHCl_3$ 18 °C): $\delta$ = 0.79 (s, 9H; 22), 0.80 (s, 9H; 26′), 0.87 (s, 9H; 24′), 1.30 (s, 9H; 26), 1.31 (s, 9H; 22′), 1.35 (s, 9H; 24), 3.21 (d, $^2J$ = 13 Hz (H, H), 4H; 3B + 3B′), 3.25 (d, $^2J$ = 13 Hz (H, H), 4H; 8B + 8B′), 4.36 (br s, 8 H, 5/6/15′/16′), 4.41 (br m, 8H; 5/6/15′/16′), 4.47 (d, $^2J$ = 13 Hz (H, H), 4H; 3B + 8B), 4.56 (d, $^2J$ = 12 Hz (H, H), 4H; 8B′ + 3B′), 4.98 (m, 2H; 16), 5.05 (m, 2H; 6′), 5.11 (m, 2H; 15), 5.20 (m, 2H; 5′), 6.47 (s, 2H; 12′), 6.48 (s, 2H; 9), 6.49 (s, 2H; 19′), 6.67 (s, 2H; 2), 7.06 (s, 2H; 12), 7.1 (s, 2H; 19), 7.11 (s, 2H; 9′), 7.44 (s, 2H; 2′); $^{13}$C NMR (75 MHz, [D]$CHCl_3$, 18 °C): $\delta$ = 30.97 (26′ + 22), 31.12 (24′), 31.66 (24), 31.69 (22′ + 26), 31.84 (3B′), 32.14 (3B + 8B′), 32.16 (8B), 33.54 (25′ + 21), 33.66 (23′), 34.10 (21′ + 25), 34.21 (23), 72.10 (5/6/6′/15′/16/16′), 72.34 (5/6/6′/15′/16/16′), 72.51 (5/6/6′/15′/16/16′), 72.66 (5/6/6′/15′/16/16′), 72.95 (15), 73.05 (5′), 84.80 (1′), 86.12 (1), 124.88 (12′), 124.91 (9), 125.06 (19′), 125.54 (9′ + 19), 125.88 (12), 130.99 (3′/13′), 131.69 (8/18), 131.74 (8/18), 134.51 (3/13), 135.08 (8′ + 18′), 136.03 (3/13), 136.92 (2), 137.22 (2′), 138.61 (3′/13′), 144.42 (10/20′), 144.45 (10/20′), 144.81 (20), 144.89 (10′), 145.04 (11′), 145.22 (11), 152.50 (7), 152.57 (17′), 152.87 (14′), 154.97 (4), 155.85 (7′/14), 156.01 (17), 158.37 (4′); MS (MALDI): *m*/*z*: 1564.28 [*M* + Na].

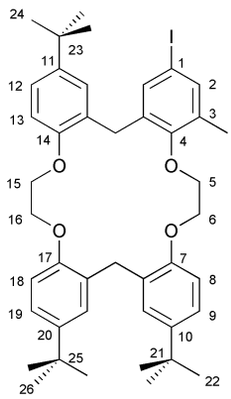


**Fig. 12** Numbering scheme for NMR assignment of calix[4]tube **14**.

## Crystallography §

Crystal Data **11**, 2.58$H_2O$, $CH_2Cl_2$, 0.5$CH_2Cl_2$, $C_{81.50}$ $H_{91.16}$ $Cl_4$ $I_4O_{11.58}$, *M* = 1905.46, triclinic, spacegroup *P*-1, *a* = 11.413(17), *b* = 13.296(17), *c* =32.14(4) Å, *α* = 81.61(1), *β* = 81.64(1), *γ* = 67.08(1)°, *U* = 4423 Å$^3$, *Z* = 2, $d_m$ = 1.431 Mg m$^{-3}$, *μ* = 1.583 mm$^{-1}$

Crystal Data **12**, 7$H_2O$, $C_{109}$ $H_{116}Br_4O_8$, *M* = 1873.66, monoclinic, space group *C*2/*c*, *a* = 32.85(4), *b* = 13.692(17), *c* = 47.55(6) Å, *β* = 98.55(1), *U* = 21151 Å$^3$, *Z* = 8, $d_m$ = 1.177 Mg m$^{-3}$, *μ* = 1.573 mm$^{-1}$.

Intensity data were collected with Mo-Kα radiation using the MARresearch Image Plate System The crystals were positioned at 90 mm from the Image Plate. 100 frames were measured at 2° intervals with a counting time of 5 min to give for **11**, 19032 reflections of which 10452 were independent (*R*(int) = 0.0523) and for **12**, 21070 reflections of which 11253 were independent (*R*(int) = 0.0910). Data analyses were carried out with the XDS program.[23] The structures were solved using direct methods with the Shelx86 program.[24] In both structures the majority of non-hydrogen atoms were refined with anisotropic thermal parameters. In **12**, some of the octyl groups appeared disordered but suitable models could not be found and atoms were refined isotropically with distance constraints. Both molecules contained several solvent molecules, many of which were disordered with reduced occupancy. The hydrogen atoms were included in geometric positions and given thermal parameters equivalent to 1.2 times those of the atom to which they were attached. Empirical absorption corrections were carried out using DIFABS.[25] The structures were refined on $F^2$ using SHELXL.[26] The final *R* values were *R*1 0.0903 and w*R*2 0.2431 for 7311 data and 0.1232, 0.3094 for 3433 data respectively,

§ CCDC reference numbers 98704. See http://www.rsc.org/suppdata/ob/b2/b211303a/ for crystallographic data in .cif or other electronic format.

both with $I > 2\sigma(I)$. The largest peaks and holes in the final different Fourier maps were 0.849, −1.116 and 0.815, −0.348 eÅ$^{-3}$ respectively.

### Computational chemistry

Gas phase MD simulations were carried out at a variety of temperatures within the NVE ensemble using Cerius 2.[27] Potential parameters for the study of $Tl^+$, $K^+$ and $Ag^+$ within calix[4]tubes were taken from the UFF[28] except for $Tl^+$ which we derived in an earlier study. The atoms in the O–$CH_2$–$CH_2$–O links were given charges taken from Ref. 29 and partial atomic charges for atoms in the calix[4]tube were calculated using the Gasteiger method and then adjusted to give a neutral tube. The metals were given a +1 charge and the charges on the calix[4]tube were kept unchanged. The time step was 1.0 fs and the simulation was carried out for 500 ps unless otherwise stated. The set of atomic positions was saved every 250 time steps (0.25 ps) leading to trajectory files with 2000 conformations.

## Acknowledgements

We thank the EPSRC for a postdoctoral fellowship (SEM) and for the use of the mass spectrometry service of the University of Wales, Swansea. The University of Reading and the EPSRC are gratefully acknowledged for funding towards the crystallographic image plate system. V. F. thanks F.C.T. for a sabbatical leave grant.

## References

1 P. Schmitt, P. D. Sheen, M. G. B. Drew and P. D. Beer, *Angew. Chem., Int. Ed. Engl.*, 1997, **36**, 1840–1842.
2 S. E. Matthews, P. Schmitt, V. Felix, M. G. B. Drew and P. D. Beer, *J. Am. Chem. Soc.*, 2002, 1341–1353.
3 S. E. Matthews, V. Felix, M. G. B. Drew and P. D. Beer, *New J. Chem.*, 2001, 1355–1358.
4 J. Buhdka, P. Lhotak, I. Stibor, V. Michlova, J. Sykova and I. Cisarova, *Tetrahedron Lett.*, 2002, **43**, 2857–2861.
5 M. Makha, P. J. Nichols, M. J. Hardie and C. L. Raston, *J. Chem. Soc., Perkin Trans. 1*, 2002, 354–359.
6 A. Notti, S. Occhipinti, S. Pappalardo, M. F. Parisi, I. Pisagatti, A. J. P. White and D. J. Williams, *J. Org. Chem.*, 2002, 7569–7572.
7 V. Felix, S. E. Matthews, P. D. Beer and M. G. B. Drew, *Phys. Chem. Chem. Phys.*, 2002, 3849–3858.
8 S. E. Matthews, V. Felix, M. G. B. Drew and P. D. Beer, *Inorg. Chem.*, 2003, **42**, 729–734.
9 S. E. Matthews and P. D. Beer, in *Calixarenes 2001*, eds. Z. Asfari, V. Böhmer, J. Harrowfield and J. Vicens, Kluwer Academic Publishers, Dordrecht, 2001.
10 (*a*) R. K. Castellano, D. M. Rudkevich and J. Rebek, *Proc. Natl. Acad, Sci. USA*, 1997, **94**, 7132–7137; (*b*) J. Rebek, *Chem. Commun.*, 2000, 637–643.
11 For general reviews on calixarenes see: (*a*) C. D. Gutsche, *Calixarenes*, The Royal Society of Chemistry, Cambridge, 1989; (*b*) V. Böhmer, *Angew. Chem., Int. Ed. Engl.*, 1995, **34**, 713–745.
12 K. D. Shimizu and J. Rebek, *Proc. Natl. Acad. Sci. USA*, 1995, **92**, 12403–12407.
13 M. Jorgensen, M. Larsen, P. SommerLarsen, W. B. Petersen and H. Eggert, *J. Chem. Soc., Perkin Trans. 1*, 1997, 2851–2855.
14 N. Kuhnert and A. LeGresley, *J. Chem. Soc., Perkin Trans. 1*, 2001, 3393–3398.
15 C. D. Gutsche and P. F. Pagoria, *J. Org. Chem.*, 1985, **50**, 5795–5802.
16 J. K. Moran, E. M. Georgiev, A. T. Yourdanov, J. T. Mague and D. M. Roundhill, *J. Org. Chem.*, 1994, **59**, 5990–5998.
17 (*a*) A. Arduini, A. Pochini, A. Rizzi, A. R. Sicuri and R. Ungaro, *Tetrahedron Lett.*, 1990, **31**, 4653–4656; (*b*) A. Arduini, A. Pochini, A. R. Sicuri, A. Secchi and R. Ungaro, *Gazz. Chim. Ital.*, 1994, **124**, 129–132.
18 Magnetisations of irradiated and exchange peak obtained from EXSY1D data at 328 K. Rates for the slow chemical exchange were calculated using CIFIT: A. D. Bain and J. A. Cramer, *J. Magn. Reson. Ser. A*, 1996, **118**, 21–27.
19 B. J. Goolsby, J. S. Brodbelt, E. Adou and M. T. Blanda, *Int. J. Mass Spectrom. Ion Processes*, 1999, **193**, 197–204; M. T. Blanda, D. B. Farmer, J. S. Brodbelt and B. J. Goolsby, *J. Am. Chem. Soc.*, 2000, **122**, 1486–1491.
20 In all plots of torsion angle against time, we have adopted the following methodology to make the plots as meaningful as possible. The default value of a torsion angle lies between −180 and +180°. However on occasion the value is changed by the addition or subtraction of 360° in order to minimise the change in angle observed in the plots. The axis range for the torsion angle is selected accordingly taking into account all torsion angles selected for the plot (Generic (*i.e.* signless) conformations are given in italics).
21 The yellow and green curves represent torsion angles from the 1,3 linkages (with O–$CH_2$–$CH_2$–O torsion angles *trans*) and the red and blue from the 2,4 linkages (with O–$CH_2$–$CH_2$–O torsion angles gauche).
22 Problems associated with microanalysis of calixarenes have previously been reported (*a*) V. Böhmer, K. Jung, M. Schön and A. Wolff, *J. Org. Chem.*, 1992, **57**, 790–792; (*b*) C. D. Gutsche and K. A. See, *J. Org. Chem.*, 1992, **57**, 4527–4539.
23 W. Kabsch, *J. Appl. Crystallogr.*, 1988, **21**, 916–924.
24 G. M. Sheldrick, *Acta Crystallogr. Sect. A Found. Crystallogr.*, 1990, **46**, 467–473.
25 G. M. Sheldrick, Shelxl, 1993, program for crystal structure refinement. University of Gottingen.
26 N. Walker and D. Stuart, *Acta Crystallogr. Sect. A Found. Crystallogr.*, 1983, **39**, 158–166.
27 Cerius2 v3.5 Molecular Simulations Inc., San Diego, USA, 1997.
28 A. K. Rappe, C. J. Casewit, K. S. Colwell, W. A. Goddard III and W. M. Skiff, *J. Am. Chem. Soc.*, 1992, **114**, 10024–10035.
29 A. Varnek and G. Wipff, *J. Comp. Chem.*, 1996, **17**, 1520–1531.